 CMES, vol.8, no.2, pp.105-117, 2005

Acoustic Scattering from Complex Shaped Three Dimensional Structures

B. Chandrasekhar[1] **and S. M. Rao**[2]

Abstract: In this work, a simple, robust, and an efficient numerical algorithm to calculate the scattered acoustic fields from complex shaped objects such as aircrafts and missiles, subjected to a plane wave incidence is presented. The work is based on the recently proposed method of moments (MoM) and the potential theory, unlike the standard Helmholtz integral equation (HIE) solution method. For the numerical solution, the scattering structure is approximated by planar triangular patches. For the MoM solution of complex bodies involving open/closed/intersecting surfaces, a unified set of basis functions to approximate the source distribution is defined. These basis functions along with suitable testing procedure generates a simple numerical algorithm applicable to complex shaped finite bodies. Finally, several numerical examples, along with comparison with other methods wherever possible, have been presented to illustrate the capabilities of the present method.

keyword: Acoustic Scattering, Method of Moments, Complex bodies.

1 Introduction

The radiation and scattering of acoustic fields by arbitrarily-shaped complex bodies such as aircrafts and missiles, surrounded by an infinite homogeneous acoustic medium is a problem of considerable interest. Although geometrical and physical theory of diffraction methods [Ufimtsev (2003)] are popular for acoustically large bodies, i.e. when the physical dimensions of the body is several wavelengths long, the boundary integral methods (BIM) are preferred solution methods for the low to medium range frequencies. For open region problems, the BIM's are even more attractive when compared to differential equation methods *viz*. finite-element methods [Ciskowski and Brebbia (1991)]. The obvious reasons are: a) the solution region is confined to the surface of the object and b) the exact enforcement of radiation condition. Although T-matrix methods have been popular to deal with such problems [Varadan and Varadan (1980)], Tobocman (1984, 1985) has demonstrated that the Helmholtz Integral Equation (HIE) method is superior for many three-dimensional scattering problems. However, the HIE solution suffers from one basic problem, *viz*. the non-uniqueness of solution at wavenumbers corresponding to the interior Dirichlet or Neumann characteristic wavenumbers. The proposed remedy, and a popular one, is the so-called CHIEF (Combined Helmholtz Integral Equation Formulation) method developed by Schenck (1968) and Benthien and Schenck (1997). Unfortunately, the CHIEF method is somewhat heuristic and prone to inaccuracies specially at high-frequencies.

As an alternative to CHIEF method, there exists another method proposed by Burton and Miller (BM) (1971) which is more elegant and mathematically guaranteed to be stable. The BM procedure basically suggests developing two separate formulations *viz*. a) HIE formulation and b) It's normal derivative, and combining these two formulations to obtain a stable solution at all frequencies. Unfortunately, the normal derivative operation results in a hyper-singular kernel which requires complicated numerical methods to solve effectively. Nevertheless, there exists a numerical algorithm, CONDOR (Composite Outward Normal Derivative Overlap Relation), developed using the BM approach, appears to be an alternative to CHIEF algorithm [Reut (1985)].

The regularization of the hyper-singular kernel and consequently a more efficient alternative to CONDOR has received considerable attention from the researchers in acoustic scattering community. The list is exhaustive and only recent works are included here for the sake of brevity [Liu and Rizzo (1992), Liu and Chen (1999), Qian, Han, Ufimtsev, and Atluri (2004b), Yan, Hung, and Zheng (2003)]. Obviously, these methods are quite successful and popular.

[1] Supercomputer Education and Research Centre, IISc, Bangalore - 560012, INDIA

[2] Department of E &CE, Auburn University, Auburn, AL-36849, USA.

Although CHIEF and CONDOR algorithms have been used extensively, neither of these methods are applicable to open bodies *i.e.* bodies with zero-thickness such as thin plates. It may be noted that, in a practical sense, everybody is a closed body. However, it is much more efficient to treat several geometrical shapes as open bodies by ignoring the finite thickness. For example, thin plates, discs and aircraft wings may be treated as open bodies, to name a few, because the thickness of such bodies is very small compared to other geometrical dimensions. Thus, for efficient modeling purposes, a general complex, arbitrary body may have open as well as closed surfaces. Hence, a practical numerical algorithm must distinguish open/closed surfaces for efficiency reasons and be able to overcome the instability problems. Unfortunately, both CHIEF and CONDOR algorithms are extremely inefficient to handle such problems. Note that similar techniques are available in the area of computational electromagnetics which resulted in extremely popular and efficient numerical algorithms [Chew, Song, Cui, Velamparambil, Hastriter, and Hu (2004), Reitich and Tamma (2004)].

Recently, Chandrasekhar and Rao (2004a, 2004b) have developed novel numerical procedures to overcome the instability problem as well as the open body problem. Further, Chandrasekhar and Rao (2004a, 2004b) based their formulation on Potential theory [Kellog (1929)] which is popularly known in acoustics as indirect method [Ciskowski and Brebbia (1991), Hwang and Chang (1991), Qian, Han, and Atluri (2004a)]. In the potential theory approach, a fictitious source distribution is assumed on the scattering/radiation surface which produces the scattered/radiated field. Uniqueness of the acoustic solution is guaranteed by enforcing the boundary conditions. However, their work presented simple canonical shapes only. In the present work, the numerical procedures are extended to handle truly arbitrary bodies under a unified algorithm which is simple and efficient. The main features of the present work are:

- Using a single formulation to work for both open and closed bodies.
- The present formulation automatically eliminates the instability problem.
- Describing and utilizing appropriate mathematical and numerical procedures for bodies involving intersecting surfaces.
- Demonstrating the applicability of the present procedure to truly arbitrary bodies.

The paper is organized as follows:

In the next section, a detailed description of the integral equation derivation is presented. In Section 3, numerical steps involved in the solving of the integral equation is detailed. The numerical procedure is based on the well-known method of moments (MoM) [Harrington (1968)] which is a popular choice for boundary integral equation solution. It may be noted that MoM has been used in several acoustic scattering problems previously [Chen, Ju, and Cha (2000), Rao and Raju (1989), Chandrasekhar and Rao (2004a, 2004b)]. In Section 4, numerical results for several example problems are presented. It may be noted that although the present formulation has been extensively tested with canonical shapes and found to be accurate, only few selected geometrical shapes are presented along with comparison with other methods for illustration purposes. Also in this section, several numerical results for complex geometries, hitherto not reported in the literature, are presented to illustrate the capabilities of the present algorithm.

2 Mathematical Formulation

Consider an arbitrarily shaped three-dimensional acoustically rigid body surrounded by an infinite, homogeneous, non-viscous medium, such as air, as shown schematically in Fig. 1. The arbitrary body is assumed to be orientable, may be open or closed, and may have intersecting surfaces.

Let S represent the surface of the body, ρ and c be the density and speed of sound in the surrounding medium, respectively. Let $(p^i, \boldsymbol{u}^i)$ and $(p^s, \boldsymbol{u}^s)$ represent the incident and scattered pressure and velocity fields, respectively. It is important to note that the incident fields are defined in the absence of the scatterer. It is customary to introduce a velocity potential Φ such that $\boldsymbol{u} = \nabla\Phi$ and $p = -j\omega\rho\Phi$, assuming harmonic time variation.

Let σ represent the simple source distribution on the scatterer. By following the approach of Burton and Miller (1971) and using the potential theory [Kellog (1929)] in conjunction with free space Green's function, the scattered velocity potential may be defined as

$$\Phi^s = \int_S \sigma(\boldsymbol{r}') \left[j\alpha G(\boldsymbol{r}, \boldsymbol{r}') + j(1-\alpha) \frac{\partial G(\boldsymbol{r}, \boldsymbol{r}')}{\partial n'} \right] ds' \quad (1)$$

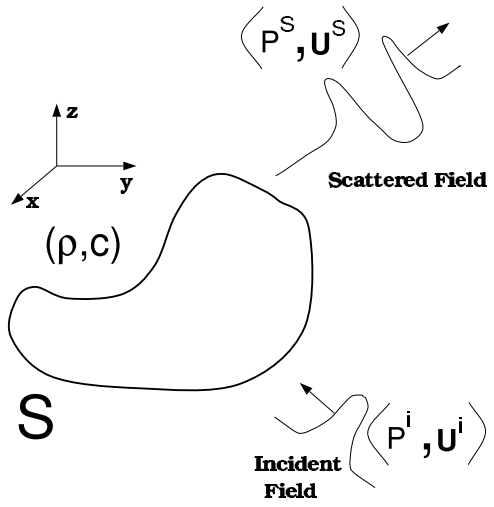

Figure 1 : Arbitrary body excited by an acoustic plane wave

where α represents a real additive constant which is chosen typically between 0 and 1. The value of α is not critical. In this work, α is set to 0 and 0.5 for open and closed bodies, respectively. Note that this choice is automated in the algorithm. The computer program thus developed, automatically checks whether the body is closed or open and sets α accordingly.

In Eq. (1)

$$G(\boldsymbol{r},\boldsymbol{r}') = \frac{e^{-jkR}}{4\pi R}, \tag{2}$$

and

$$R = \left|\boldsymbol{r}-\boldsymbol{r}'\right|, \tag{3}$$

$\boldsymbol{r}'$, $\boldsymbol{r}$ and k represent the locations of the source point, location of the observation point, and the wave number, respectively. Both $\boldsymbol{r}$ and $\boldsymbol{r}'$ are defined with respect to a global coordinate origin O. Also, note that in Eq. (1), $\partial/\partial n'$ represents the normal derivative with respect to the source point $\boldsymbol{r}'$. Noting that, at the surface of the hard scatterer, normal derivative of the total velocity potential, which is the sum of the incident and scattered potentials must vanish, the integral equation may be derived, given by

$$\begin{aligned}\int_S \sigma(\boldsymbol{r}')\left[j\alpha\frac{\partial G(\boldsymbol{r},\boldsymbol{r}')}{\partial n}+j(1-\alpha)\frac{\partial}{\partial n}\frac{\partial G(\boldsymbol{r},\boldsymbol{r}')}{\partial n'}\right]ds' \\ = -\frac{\partial \Phi^i(\boldsymbol{r})}{\partial n},\end{aligned} \tag{4}$$

where $\partial/\partial n$ represents the normal derivative with respect to the observation point $\boldsymbol{r}$. Further, in Eq. (4), Φ^i represents the incident velocity potential which is related to the incident pressure field p^i by the relation $p^i = -j\omega\rho\Phi^i$.

Next, following the procedures described in [Maue (1949) and Mitzner (1966)], Eq. (4) may be re-written as

$$\begin{aligned}&j\alpha\int_S \sigma(\boldsymbol{r}')\frac{\partial G(\boldsymbol{r},\boldsymbol{r}')}{\partial n}\,ds' \\ &+j(1-\alpha)\int_S \boldsymbol{a}_n\bullet\boldsymbol{a}_n' k^2\,\sigma G ds' \\ &+j(1-\alpha)\int_S \left(\boldsymbol{a}_n'\times\nabla'\sigma\right)\bullet\left(\boldsymbol{a}_n\times\nabla G\right)ds' \\ &=\boldsymbol{a}_n\bullet\nabla\Phi^i\end{aligned} \tag{5}$$

where $\boldsymbol{a}_n$ and $\boldsymbol{a}_n'$ represent the unit normal vectors at $\boldsymbol{r}$ and $\boldsymbol{r}'$, respectively. Also, the prime on the ∇ operator refers to the differentiation with respect to primed coordinates only.

3 Numerical Solution Procedure

In this section, the numerical solution to solve Eq. (5) is detailed using MoM. Although the MoM procedure is well-known, for the sake of completeness only a short review is presented here.

Consider the deterministic equation

$$\boldsymbol{L}\boldsymbol{f} = \boldsymbol{g}, \tag{6}$$

where $\boldsymbol{L}$ is a linear operator, $\boldsymbol{g}$ is a known function and $\boldsymbol{f}$ is an unknown function to be determined. Let $\boldsymbol{f}$ be represented by a set of known functions $\boldsymbol{f}_j,\ j = 1,2,.....,N$, termed as basis functions in the domain of $\boldsymbol{L}$ as a linear combination, given by

$$\boldsymbol{f} = \sum_{j=1}^{N}\alpha_j\boldsymbol{f}_j, \tag{7}$$

where α_j are scalar coefficients to be determined. Substituting Eq. (7) into Eq. (6), and using the linearity of $\boldsymbol{L}$, we have

$$\sum_{j=1}^{N}\alpha_j\boldsymbol{L}\boldsymbol{f}_j = \boldsymbol{g}, \tag{8}$$

where the equality is usually approximate. Let $(\boldsymbol{w}_1,\boldsymbol{w}_2,\boldsymbol{w}_3,....)$ define a set of testing functions in the

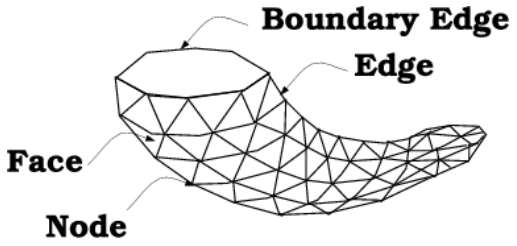

Figure 2 : Arbitrary body modeled by triangular patches

range of $\boldsymbol{L}$. Now, taking the inner product of Eq. (8) with each $\boldsymbol{w}_i$ and using the linearity of inner product defined as $\langle \boldsymbol{f}, \boldsymbol{g} \rangle = \int_s \boldsymbol{f} \cdot \boldsymbol{g}\, ds$, we obtain a set of linear equations, given by

$$\sum_{j=1}^{N} \alpha_j \langle \boldsymbol{w}_i, , \boldsymbol{L}\boldsymbol{f}_j \rangle = \langle \boldsymbol{w}_i, \boldsymbol{g} \rangle , \quad i = 1,2,3....,N \tag{9}$$

The set of equations in Eq. (9) may be written in the matrix form as

$$\boldsymbol{Z}\boldsymbol{X} = \boldsymbol{Y}, \tag{10}$$

which can be solved for $\boldsymbol{X}$ using any standard linear equation solution methodologies.

Although, the MoM is conceptually very simple, the simplicity of the method lies in defining the appropriate basis functions and applying suitable numerical procedures. For the problem at hand, note that the unknown quantity to be evaluated is σ.

3.1 Derivation of Matrix Equations

First of all, approximate the arbitrary body using planar triangular patch modeling. The body is assumed to be connected, orientable, of finite extent, and may be composed of intersecting surfaces. In general, a triangulated surface modeling an arbitrary body consists of N_f planar triangular faces, N_v vertices, and N_e edges. These geometrical elements are illustrated in Fig. 2. The triangular patch modeling is the most efficient way of describing an arbitrary body to the digital computer. Further, there exist a variety of mesh generation codes which can be effectively used for the present numerical scheme.

Next, it is convenient to start the development of basis functions to represent the unknown quantity σ by noting that each basis function is to be associated with an interior edge. Note that the interior edge is an edge which has at-least two triangles (more than two triangles for intersecting bodies) connected to it.

Consider the case where exactly two triangles are connected to an interior edge. For this case, the basis function associated with the n^{th} edge is

$$f_n(\boldsymbol{r}) = \begin{cases} 1, & \boldsymbol{r} \in S_n, \\ 0, & \text{otherwise} \end{cases} \tag{11}$$

where S_n represents the region obtained by connecting the centroids of the two triangles $T_n^{\pm}$ attached to n^{th} edge, to the nodes of edge n. Note that the assignment of $\pm$ designation is arbitrary.

Now, consider the case where more than two triangles connected to a given edge. Note that when m triangles are connected to a given edge, the number basis functions associated with that edge are $m-1$. Thus, to discuss multiple basis functions that are associated with an edge, first look at the ordering scheme for multiple triangles attached to an edge. Fig. 3a illustrates an edge with three attached faces. The faces attached to this edge are numbered F_a, F_b, and F_c. For this case, since three triangles are connected to the given edge, one may define two basis functions involving (F_a, F_b) and (F_a, F_c) as shown in Fig. 3b and Fig. 3c. Note that this discussion readily generalizes to edges with arbitrary multiplicity.

Using these basis functions, the unknown source distribution σ may be approximated as

$$\sigma(\boldsymbol{r}) \;=\; \sum_{n=1}^{N} x_n f_n(\boldsymbol{r}) \tag{12}$$

where x_n represents the unknown coefficient to be determined. In Eq. (12), N represents the total number of basis functions, given by

$$N \;=\; \sum_{i=1}^{N_e} P_i - 1 \tag{13}$$

where P_i is the total number of patches connected to i^{th}-edge in the triangulation scheme.

Next, the testing procedure begins with defining symmetric product as

$$< f_1, f_2 >= \int_S f_1 \;\; f_2 \;\; ds \tag{14}$$

where f_1 and f_2 are two scalar functions defined over a

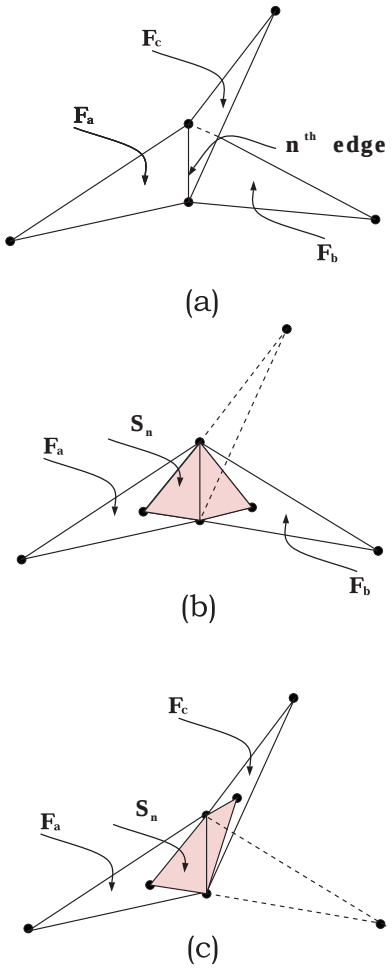

Figure 3 : Basis function for an intersecting surface

surface S. Thus, the testing equation may be written as

$$\begin{aligned} &< f_m, j\alpha \int_S \sigma(\boldsymbol{r}') \frac{\partial G(\boldsymbol{r},\boldsymbol{r}')}{\partial n} ds' > \\ &\quad + j(1-\alpha)\left[< f_m, \int_S \boldsymbol{a}_n \bullet \boldsymbol{a}'_n k^2 \sigma G ds' > \right. \\ &\quad \left. + < f_m, \int_S \left(\boldsymbol{a}'_n \times \nabla\sigma\right) \bullet (\boldsymbol{a}_n \times \nabla G)\, ds' > \right] \\ &= < f_m, \boldsymbol{a}_n \bullet \nabla \Phi^i > . \end{aligned} \tag{15}$$

In the following, each term in Eq. (15) is evaluated. Considering the evaluation of first term in Eq. (15), given by

$$\begin{aligned} &< f_m, \int_S \sigma(\boldsymbol{r}') \frac{\partial G(\boldsymbol{r},\boldsymbol{r}')}{\partial n} ds' > \\ &\quad = \int_{S_m^+} \int_S \sigma(\boldsymbol{r}') \frac{\partial G(\boldsymbol{r},\boldsymbol{r}')}{\partial n} ds' ds \\ &\quad + \int_{S_m^-} \int_S \sigma(\boldsymbol{r}') \frac{\partial G(\boldsymbol{r},\boldsymbol{r}')}{\partial n} ds' ds \\ &\quad \approx \frac{A_m^+}{3} \int_S \sigma(\boldsymbol{r}') \frac{\partial G(\boldsymbol{r}_m^+,\boldsymbol{r}')}{\partial n} ds' \\ &\quad + \frac{A_m^-}{3} \int_S \sigma(\boldsymbol{r}') \frac{\partial G(\boldsymbol{r}_m^-,\boldsymbol{r}')}{\partial n} ds' \end{aligned} \tag{16}$$

where $\boldsymbol{r}_m^\pm$ represents the position vector to the centroid of $S_m^\pm$ and $A_m^\pm$ is the area of the triangle $T_m^\pm$. Note that the double surface integration in Eq. (16) is approximated as a single integral by evaluating the integrand at the centroids of respective triangles $S_m^\pm$as illustrated in [Chandrasekhar and Rao (2004)]. Thus, the Eq. (16) can be written as

$$\begin{aligned} &< f_m, \int_S \sigma(\boldsymbol{r}') \frac{\partial G(\boldsymbol{r},\boldsymbol{r}')}{\partial n} ds' > \\ &\quad \approx \frac{A_m^+}{3} \left[\frac{\sigma(\boldsymbol{r}_m^+)}{2} - \int\!\!\!\!\!\!- _S \sigma(\boldsymbol{r}') \frac{\partial G(\boldsymbol{r}_m^+,\boldsymbol{r}')}{\partial n} ds' \right] \\ &\quad + \frac{A_m^-}{3} \left[\frac{\sigma(\boldsymbol{r}_m^-)}{2} - \int\!\!\!\!\!\!- _S \sigma(\boldsymbol{r}') \frac{\partial G(\boldsymbol{r}_m^-,\boldsymbol{r}')}{\partial n} ds' \right] \end{aligned} \tag{17}$$

where $\int\!\!\!\!\!\!-_S$ represents the integration over the surface excluding the principal value term *i.e.* $\boldsymbol{r} = \boldsymbol{r}'$. Note that the $\int\!\!\!\!\!\!-_S$ represents a well-behaved integral which can be trivially evaluated using standard integration algorithms [Wilton Rao, Glisson, Schaubert, Al-Bundak, and Butler (1984), Hammer, Marlowe, and Stroud (1956)].

Next, consider

$$\begin{aligned} &< f_m, \int_S \boldsymbol{a}_n \bullet \boldsymbol{a}'_n k^2 \sigma G ds' > \\ &= \int_S f_m(\boldsymbol{r}) \int_S \boldsymbol{a}_n \bullet \boldsymbol{a}'_n k^2 \sigma(\boldsymbol{r}') G(\boldsymbol{r},\boldsymbol{r}')\, ds'\ ds \\ &\approx \left(\frac{A_m^+}{3} \boldsymbol{a}_m^+ + \frac{A_m^-}{3} \boldsymbol{a}_m^- \right) \bullet \int_S \boldsymbol{a}'_n k^2 \sigma(\boldsymbol{r}') G(\boldsymbol{r}_m,\boldsymbol{r}') ds' \end{aligned} \tag{18}$$

where $\boldsymbol{a}_m^\pm$ and $\boldsymbol{r}_m$ represents the unit normal vectors of the triangles connected to the m^{th}-edge and the position vector to the mid-point of the m^{th}-edge, respectively. Note that the double surface integration in Eq. (18) is converted to single surface integral by approximating the integrand at the center of the m^{th}-edge and multiplying by the area of the sub-domain patch, as done for Eq. (16).

Next, using the same logic and assuming the incident field to be a slowly varying function, the right hand side of Eq. (15) may be approximated as

$$\begin{aligned} &< f_m, \boldsymbol{a}_n \bullet \nabla\Phi^i >= \int_S f_m(\boldsymbol{r}) \boldsymbol{a}_n \bullet \nabla\Phi^i(\boldsymbol{r}) ds \\ &\approx \left(\frac{A_m^+}{3} \boldsymbol{a}_m^+ + \frac{A_m^-}{3} \boldsymbol{a}_m^- \right) \bullet \nabla\Phi^i(\boldsymbol{r}_m) \end{aligned} \tag{19}$$

Now, consider the evaluation of $< f_m, \int_S (\boldsymbol{a}_n' \times \nabla\sigma) \bullet (\boldsymbol{a}_n \times \nabla G)\, ds' >$ term in Eq. (15). Following the numerical procedure developed in [Chandrasekhar and Rao (2004a), we have

$$\begin{aligned} &< f_m, \int_S \left(\boldsymbol{a}_n' \times \nabla\sigma\right) \bullet (\boldsymbol{a}_n \times \nabla G)\, ds' > \\ &\quad = \int_S \boldsymbol{a}_n \bullet \nabla \times \boldsymbol{A}\, ds \\ &\quad = \oint_{C_m} \boldsymbol{A} \bullet \boldsymbol{dl} \\ &\quad \approx \boldsymbol{\ell}_m \bullet \left[\boldsymbol{A}(\boldsymbol{r}_m^{c-}) - \boldsymbol{A}(\boldsymbol{r}_m^{c+}) \right] \end{aligned} \tag{20}$$

where

$$A = \int_S \left(\boldsymbol{a}_n' \times \nabla\sigma\right)\ G\, ds', \tag{21}$$

C_m and $\boldsymbol{\ell}_m$ are the contour of the basis function and the vector along the length associated with the m^{th}-edge, respectively.

Finally, combining Eqs. (17), (18), (19), and (20), the testing equation Eq. (15) may be written as

$$\begin{aligned} &j\alpha \frac{A_m^+}{3} \left\{ \frac{\sigma(\boldsymbol{r}_m^+)}{2} - \int_S \sigma(\boldsymbol{r}') \frac{\partial G(\boldsymbol{r}_m^+, \boldsymbol{r}')}{\partial n}\, ds' \right\} \\ &+ j\alpha \frac{A_m^-}{3} \left\{ \frac{\sigma(\boldsymbol{r}_m^-)}{2} - \int_S \sigma(\boldsymbol{r}') \frac{\partial G(\boldsymbol{r}_m^-, \boldsymbol{r}')}{\partial n}\, ds' \right\} \\ &+ j(1-\alpha) \left\{ \boldsymbol{\ell}_m \bullet \left[\boldsymbol{A}(\boldsymbol{r}_m^{c-}) - \boldsymbol{A}(\boldsymbol{r}_m^{c+}) \right] \right. \\ &+ \left. \left(\frac{A_m^+}{3} \boldsymbol{a}_m^+ + \frac{A_m^-}{3} \boldsymbol{a}_m^- \right) \bullet \int_S \boldsymbol{a}_n' k^2 \sigma(\boldsymbol{r}') G(\boldsymbol{r}_m, \boldsymbol{r}') ds' \right\} \\ &= \left(\frac{A_m^+}{3} \boldsymbol{a}_m^+ + \frac{A_m^-}{3} \boldsymbol{a}_m^- \right) \bullet \nabla\Phi^i(\boldsymbol{r}_m) \end{aligned} \tag{22}$$

for $m = 1, 2, \cdots, N$. Substituting the source expansion Eqs. (12) into Eq. (22) yields an $N \times N$ system of linear equations which may be written in matrix form as

$$\boldsymbol{ZX} = \boldsymbol{Y} \tag{23}$$

where $\boldsymbol{Z} = [Z_{mn}]$ is an $N \times N$ matrix and $\boldsymbol{X} = [X_n]$ and $\boldsymbol{Y} = [Y_m]$ are column vectors of length N. Elements of $\boldsymbol{Z}$-matrix are given by

$$\begin{aligned} Z_{mn} =& j\alpha \left\{ \frac{1}{2} \left[\frac{A_m^+ + A_m^-}{3} \right] - G_{mm}^+ - G_{mm}^- \right\} \\ &+ j(1-\alpha)\, k^2 \left(\frac{A_m^+}{3} \boldsymbol{a}_m^+ + \frac{A_m^-}{3} \boldsymbol{a}_m^- \right) \bullet \boldsymbol{f}_{mn} \\ &+ j(1-\alpha) \boldsymbol{\ell}_m \bullet \left[\boldsymbol{A}_{mm}^{c-} - \boldsymbol{A}_{mm}^{c+} \right] \end{aligned} \tag{24}$$

when $m = n$ and

$$\begin{aligned} Z_{mn} =& - j\alpha \left\{ G_{mn}^+ + G_{mn}^- \right\} \\ &+ j(1-\alpha)\, k^2 \left(\frac{A_m^+}{3} \boldsymbol{a}_m^+ + \frac{A_m^-}{3} \boldsymbol{a}_m^- \right) \bullet \boldsymbol{f}_{mn} \\ &+ j(1-\alpha) \boldsymbol{\ell}_m \bullet \left[\boldsymbol{A}_{mn}^{c-} - \boldsymbol{A}_{mn}^{c+} \right] \end{aligned} \tag{25}$$

when $m \neq n$. Further,

$$Y_m = \left(\frac{A_m^+}{3} \boldsymbol{a}_m^+ + \frac{A_m^-}{3} \boldsymbol{a}_m^- \right) \bullet \nabla\Phi^i(\boldsymbol{r}_m) \tag{26}$$

In Eqs. (24), (25), and (26),

$$\boldsymbol{f}_{mn} = \boldsymbol{a}_n^+ \int_{S_n^+} \frac{e^{-jkR_m}}{4\pi R_m} ds' + \boldsymbol{a}_n^- \int_{S_n^-} \frac{e^{-jkR_m}}{4\pi R_m} ds' \tag{27}$$

$$G_{mn}^{\pm} = \frac{A_m^{\pm}}{3} \left[\int_{S_n^+} \frac{\partial G(\boldsymbol{r}_m^{\pm}, \boldsymbol{r}')}{\partial n^{\pm}} ds' \int_{S_n^-} \frac{\partial G(\boldsymbol{r}_m^{\pm}, \boldsymbol{r}')}{\partial n^{\pm}} ds' \right] \tag{28}$$

$$\boldsymbol{A}_{mn}^{c\pm} = \boldsymbol{\ell}_n \left[\frac{1}{A_n^+} \int_{T_n^+} \frac{e^{-jkR_m^{c\pm}}}{4\pi R_m^{c\pm}} ds' + \frac{1}{A_n^-} \int_{T_n^-} \frac{e^{-jkR_m^{c\pm}}}{4\pi R_m^{c\pm}} ds' \right] \tag{29}$$

$$R_m = |\boldsymbol{r}_m - \boldsymbol{r}'| \tag{30}$$

$$R_m^{c\pm} = |\boldsymbol{r}_m^{c\pm} - \boldsymbol{r}'| \tag{31}$$

Integrals, appearing in Eqs. (27) and (29), are straight forward integrals over a triangular region. However, it is cautioned that the integrals have singular kernels and, for accurate solution, may be evaluated using the methods described in [Wilton Rao, Glisson, Schaubert, Al-Bundak, and Butler (1984), Hammer, Marlowe, and Stroud (1956)].

For the plane wave incidence, set

$$\Phi^i = e^{jk\boldsymbol{k}\cdot\boldsymbol{r}} \tag{32}$$

where the propagation vector $\boldsymbol{k}$ is

$$\boldsymbol{k} = \sin\theta_o \cos\phi_0 \boldsymbol{a}_x + \sin\theta_o \sin\phi_0 \boldsymbol{a}_y + \cos\theta_o \boldsymbol{a}_z \tag{33}$$

and (θ_0, ϕ_0) defines the angle of incidence of the plane wave in terms of the usual spherical coordinate convention.

Once the elements of the moment matrix $\bar{\boldsymbol{Z}}$ and the forcing vector $\boldsymbol{Y}$ are determined, one may solve the resulting system of linear equations, Eq. (23), for the unknown column vector $\boldsymbol{X}$.

3.2 Near-Field Calculation

Once the source distribution on the object is known, the scattered velocity potential at any point in space may be calculated using Eq. (1). Obviously, for the near-field calculation *i.e.* at any point whose furtherest distance from the scatterer is small compared to wavelength, the integrals in Eq. (1) may be evaluated using the numerical procedures developed in [Wilton Rao, Glisson, Schaubert, Al-Bundak, and Butler (1984), Hammer, Marlowe, and Stroud (1956)]. Note that, although the integrals involved are not singular the evaluation of these must be done carefully to obtain accurate results. However in the following, a simple numerical procedure is presented to calculate the near-fields which may be sufficient for many situations.

Let P denote the point of observation and let $\boldsymbol{r}$ represent the the position vector to P. Then, using Eq. (1), Φ^s may be written as

$$\begin{aligned}
\Phi^s(\boldsymbol{r}) &= \int_S \sigma(\boldsymbol{r}') \left[j\alpha G(\boldsymbol{r},\boldsymbol{r}') + j(1-\alpha)\frac{\partial G(\boldsymbol{r},\boldsymbol{r}')}{\partial n'} \right] ds' \\
&\approx \sum_{n=1}^{N} \sigma_n \left[\frac{j\alpha}{3} \left\{ G(\boldsymbol{r},\boldsymbol{r}_n^{c+}) A_n^+ + G(\boldsymbol{r},\boldsymbol{r}_n^{c-}) A_n^- \right\} \right. \\
&\left. + \frac{j(1-\alpha)}{3} \left\{ \frac{\partial G(\boldsymbol{r},\boldsymbol{r}_n^{c+})}{\partial n^+} A_n^+ + \frac{\partial G(\boldsymbol{r},\boldsymbol{r}_n^{c-})}{\partial n^-} A_n^- \right\} \right]
\end{aligned} \tag{34}$$

where $\boldsymbol{r}_n^{c\pm}$ represents the position vector to the centroid of $S_n^{\pm}$. Note that since σ_n is known, one can evaluate the expression Eq. (34) very easily.

3.3 Far-Field Calculation

For the far-field calculation, it is common to assume the observation point $r \to \infty$, and, hence, the following procedure may be adopted which is fast and simple.

First of all, note that, for a far-field observation point,

$$\begin{aligned}
R = |\boldsymbol{r} - \boldsymbol{r}'| &= \left[r^2 + r'^2 - 2\,\boldsymbol{r}\cdot\boldsymbol{r}' \right]^{\frac{1}{2}} \\
&\approx r \left[1 \; - \; 2 \; \frac{\boldsymbol{r}\cdot\boldsymbol{r}'}{r^2} \right]^{\frac{1}{2}} \\
&\approx r - \boldsymbol{a}_r \cdot \boldsymbol{r}',
\end{aligned}$$

$$G(\boldsymbol{r},\boldsymbol{r}') = \frac{e^{-jkR}}{4\pi R} \approx \frac{e^{-jkr}}{4\pi r} \; e^{jk\boldsymbol{a}_r\cdot\boldsymbol{r}'} \tag{35}$$

and

$$\begin{aligned}
\frac{\partial G(\boldsymbol{r},\boldsymbol{r}')}{\partial n'} &= \frac{1+jkR}{R^2} \; \frac{e^{-jkR}}{4\pi R} \left[\boldsymbol{a}_n' \cdot (\boldsymbol{r} - \boldsymbol{r}') \right] \\
&\approx \frac{e^{-jkr}}{4\pi r} \, e^{jk\boldsymbol{a}_r\cdot\boldsymbol{r}'} \left(jk\boldsymbol{a}_n' \cdot \boldsymbol{r}' \right)
\end{aligned} \tag{36}$$

Thus, for far-field observation point, Eq. (1) may be written as

$$\begin{aligned}
\Phi^s &= \frac{e^{-jkr}}{4\pi r} \times \int_S \sigma(\boldsymbol{r}') j \left\{ \alpha + [(1-\alpha)] \left[jk\boldsymbol{a}_n' \cdot \boldsymbol{r}' \right] \right\} e^{jk\boldsymbol{a}_r\cdot\boldsymbol{r}'} ds' \\
&= \frac{e^{-jkr}}{4\pi r} \int_S \sigma(\boldsymbol{r}') \left\{ j\alpha - k(1-\alpha)\boldsymbol{a}_n' \cdot \boldsymbol{r}' \right\} e^{jk\boldsymbol{a}_r\cdot\boldsymbol{r}'} ds'
\end{aligned} \tag{37}$$

Next, utilizing Eq. (12), the far-scattered velocity potential may be written as

$$\begin{aligned}
\Phi^s &= \frac{e^{-jkr}}{4\pi r} \sum_{n=1}^{N} x_n \times \int_{S_n} \left\{ j\alpha - k(1-\alpha)(\boldsymbol{a}_n' \cdot \boldsymbol{r}') \right\} e^{jk\boldsymbol{a}_r\cdot\boldsymbol{r}'} ds' \\
&= \frac{e^{-jkr}}{4\pi r} \sum_{n=1}^{N} x_n \left(\frac{A_n^+ + A_n^-}{3} \right) \\
&\quad \times \left\{ j\alpha - k(1-\alpha)(\boldsymbol{a}_n^+ + \boldsymbol{a}_n^-) \cdot \boldsymbol{r}_n \right\} e^{jk\boldsymbol{a}_r\cdot\boldsymbol{r}_n}
\end{aligned} \tag{38}$$

Finally, scattering cross section S may be defined as

$$S = 4\pi r^2 \left| \frac{\Phi^s}{\Phi^i} \right|^2 \tag{39}$$

assuming $|\Phi^i| = 1$.

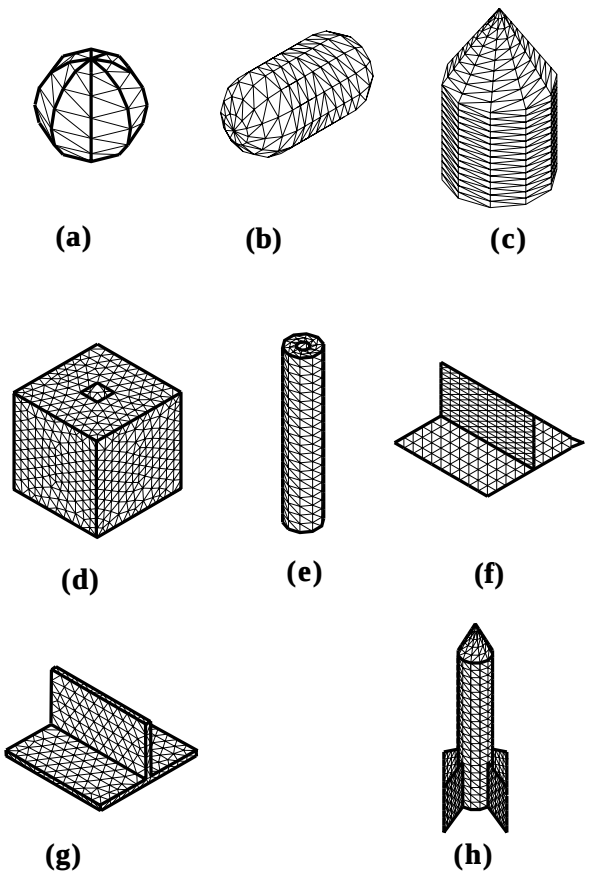

Figure 4 : Complex bodies modeled with triangular patches

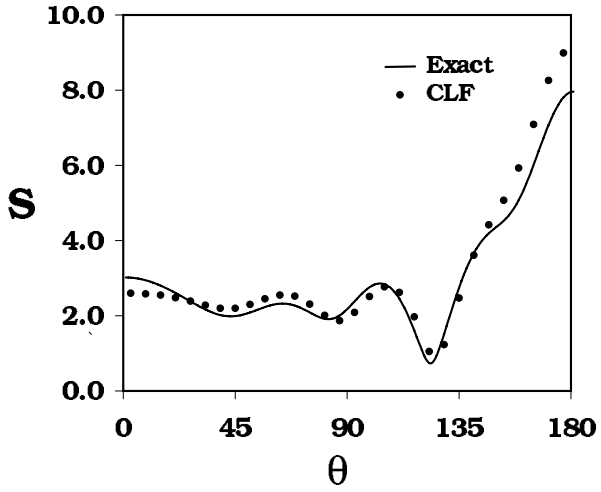

Figure 5 : Scattering cross section versus polar angle for an acoustically hard sphere ($ka = 5$)subjected to an axially incident plane wave

4 Numerical results

In this section, numerical examples for a few complex bodies depicted in Fig 4 are presented. It may be noted that the present formulation has been extensively tested with canonical shapes and found to be accurate in each case. Only few selected geometrical shapes are presented here for illustration purposes. However, the present algorithm has not been optimized and hence not compared with other standard methods such as CONDOR or CHIEF for efficiency purposes.

As a first example, consider a spherical body ($ka = 5.0$), as shown in Fig. 4a excited by an axially incident plane wave. Fig. 5 shows the far-field scattering cross section S as a function of the polar angle θ and compared with the exact solution [Bowman, Senior and Uslenghi (1969)]. The sphere is modeled by 760 triangular patches resulting in 1140 edges. The modeling is done by first dividing the θ and ϕ directions into 20 equal segments each which results in triangular patches at the sphere caps and quadrilateral patches in between. By joining the diagonal of the quadrilateral patch, the triangular discretization may be obtained. Note a good comparison between the exact solution and the present method.

As a next example, consider again a sphere ($ka = 2.0$) excited by an axially incident plane wave. In this example, convergence of the numerical solution is investigated. Fig. 6 shows the far-field scattering cross section S as a function of the polar angle θ and compared with the exact solution [Bowman, Senior, and Uslenghi (1969)]. In this figure, three cases of the numerical solution is presented with the number of unknowns 396, 630, and 1140 and compared with the exact solution. Note that the accuracy of the solution improves as the number of unknowns are increased.

Next, consider a circular cylinder with spherical end caps as shown in Fig. 4b subjected to an axially incident plane wave with wavelength equal to 2π meters. The object is placed at the center of the coordinate system with the cylinder axis coinciding with the x-axis. The radius and lengths of the cylinder are 0.5m and 2.0m, respectively. Fig. 7 shows the far-field scattering cross section S as a function of the polar angle θ in the xz-plane (i.e. $\phi = 0$) and compared with the numerical solution [Rao and Raju (1989)] using triangular patches as unknowns.The sphere-cylinder body is approximated by 360 triangular patches resulting in 540 unknowns. It is evident from the

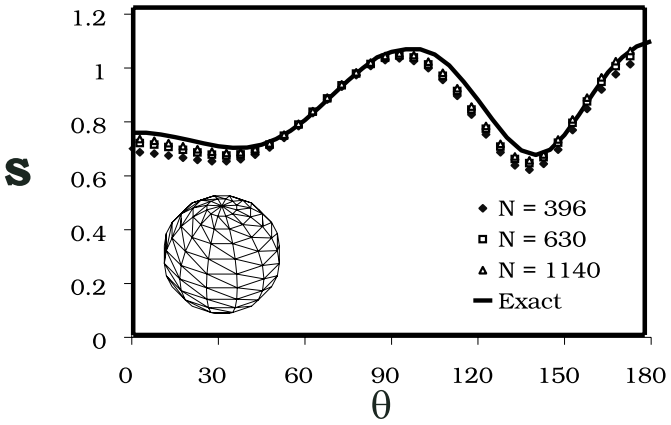

Figure 6 : Scattering cross section versus polar angle for an acoustically hard sphere ($ka = 2$) subjected to an axially incident plane wave

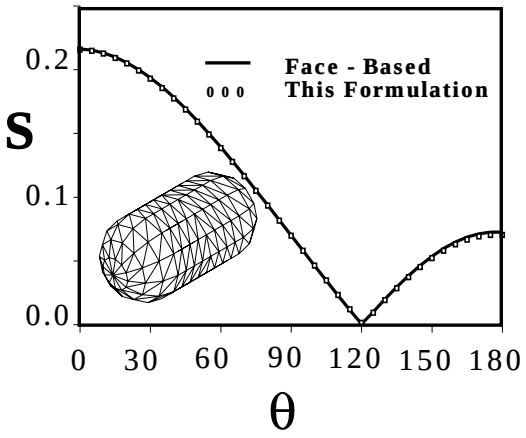

Figure 7 : Scattering cross section versus polar angle for an acoustically hard cylinder with spherical end caps subjected to an axially incident plane wave

figure that both solutions compare very well.

Next, consider a cone-cylinder as shown in Fig. 4c subjected to an axially incident plane wave. The cone-sphere is approximated by 560 triangular patches. The cylinder is 4m long, closed at one end by a circular plate of radius 2m and the other end connected to a cone of length 3m. The body is with the center of the base coinciding with the origin. The wavelength of the incident acoustic plane wave is 2πm. Fig. 8 shows the far-field scattering cross section S as a function of the polar angle θ in the xz-plane (i.e. $\phi = 0$). For comparison, again the numerical solution obtained by triangular patch solution [Rao and Raju (1989)] is also presented. Note that both solutions compare well with each other.

In the following, numerical results for several complex body shapes are presented without comparing with other methods basically because no results are available for such geometrical shapes in open literature. It may be noted that these examples are carefully selected to highlight the capabilities of the present method. If one attempts to solve these problems using CHIEF or CONDOR, the methods either fail or extremely expensive. The simple reason being the open surfaces have to be modeled as closed structures using extremely small triangles.

Consider a cube with a small aperture at the top face as shown in Fig. 4d. This particular example highlights the present algorithm's capability to handle open bodies. It may be noted that every practically realizable body has certain finite thickness associated with the surface and hence can be modeled as a closed body by placing triangles on both sides of the surface. However, it is very inefficient to do so, specially when the thickness is very small. In these cases, it may be prudent to treat the body as on open body. The side of the cube is 1m and the aperture is 0.2m$\times$ 0.2m. The cube is placed at the center of the coordinate origin and excited by an axially incident plane wave. For the numerical solution, the cube is approximated by 1348 triangles resulting in 2026 edges. Fig. 9 shows the scattering cross section as a function of polar angle θ for this case. Also, for comparison, the case of a closed cube is also presented. Here, note that the scattering cross section remains same for both cases. Intuitively this makes sense because for the observer at infinity both cases appear same.

As a next example, consider a long cylinder, 1m length and 0.1m radius, with a circular aperture of 0.03m radius on the top face as shown in Fig. 4e. The cylinder is placed with the center of the base at the origin and the axis coinciding with the z-axis of the Cartesian coordinate system. The cylinder is excited by an incoming plane wave ($k = 1\ m^{-1}$) traveling at 15° angle with respect to the z-axis. In Fig. 10, the total field, which is the sum of the incident and scattered fields, along the polar axis is presented. Notice the large value of the field within the cylinder ($z \leq 1$) and a slowly decaying field outside ($z > 1$). The large field is due to the effect of

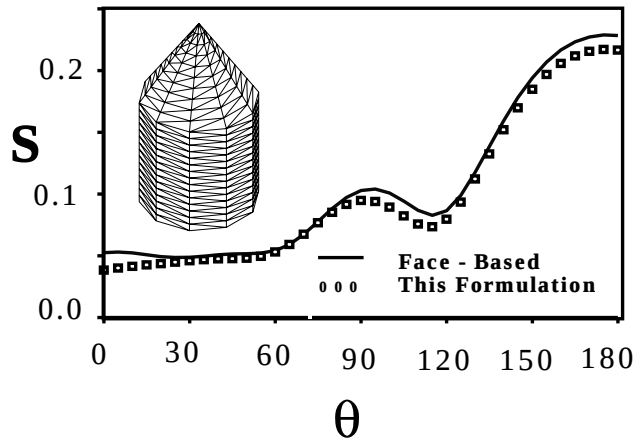

Figure 8 : Scattering cross section versus polar angle for an acoustically hard cone-cylinder subjected to an axially incident plane wave

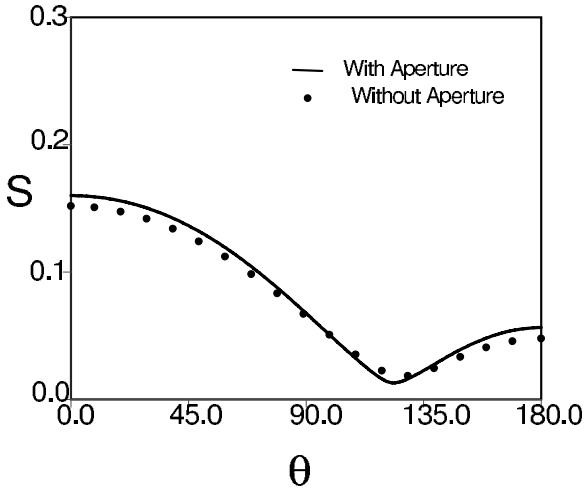

Figure 9 : Scattering cross section versus polar angle for an acoustically hard cube with an aperture subjected to an axially incident plane wave.

the cavity acting as a resonator. For numerical purposes the cylinder is modeled by 490 triangles resulting in 740 edges. It may be noted that the geometry presented in this example is not easily amenable to either CHIEF or CONDOR algorithms since the surface grid must encompass outside surface, inside surface as well as along the thick wall.

Next, consider the geometry of an infinitely thin, intersecting plate as shown in Fig. 4f. The horizontal square plate, length 1m, is intersected at the center by a vertical plate of 1m length and 0.5m height. The entire structure is placed in the Cartesian coordinate system such that the origin coincides with the center of the horizontal plate and impinged upon by an incoming, z-traveling plane wave ($k = 1\ m^{-1}$). The entire body is modeled by 400 triangular patches resulting in 630 edges. The scattering cross section S as a function of polar angle θ is presented in Fig. 11. For comparison, the solution using the method described in [Rao and Raju (1989)] is also presented. Since the algorithm described Rao and Raju (1989) is valid only for closed bodies, assume a finite thickness for the plates as shown in Fig. 4g. The triangular patch model for this geometry involves 822 patches. In the Fig. 11 the results for thickness $t = 0.01$m and $t = 0.002$m are presented. Note from Fig. 11 that as the thickness is reduced the result compares better with the present solution method. Also, note that the thick plate model involves triangles with high aspect ratio and hence is not a good model. Unfortunately, if a better model involving more or less equal area triangles is desired, then the number of triangles are too large and requires enormous computer resources.

Next, consider a missile-like structure as shown in Fig. 4h. The structure has a conical front-end backed by a cylinder. Further, four infinitely-thin fins are attached to the cylinder. The length and radius of the cylinder are 10m and 1m, respectively. The conical section is 2m long. The fins are 2.5m$\times$ 3m rectangular plates attached at the base. The triangulation of this body results in 1288 edges. The structure is placed in the Cartesian coordinate system such that the origin coincides with the center of the circular base. Fig 12 shows the scattered cross section as a function of polar angle θ when the body is excited by an acoustic plane wave with $k = 1\ m^{-1}$.

Finally, consider an aircraft modeled by triangular patches as shown in Fig 4. The aircraft is placed such that the x-axis runs along the nose direction and y-axis along the wings. The aircraft dimensions are 9.4m, 7.0m, and 2.75m along x, y, z-directions, respectively. The aircraft is modeled by 1982 triangular patches resulting in 2673 edges. Here two cases are considered. In the first case, the acoustic plane wave, at 100-Hz frequency, traveling along the z-axis is incident on the body and Fig 14 shows the scattering cross section as a function of the polar angle θ. In the second case, the plane wave, traveling along the x-axis, is incident from the nose side. In Fig 15,

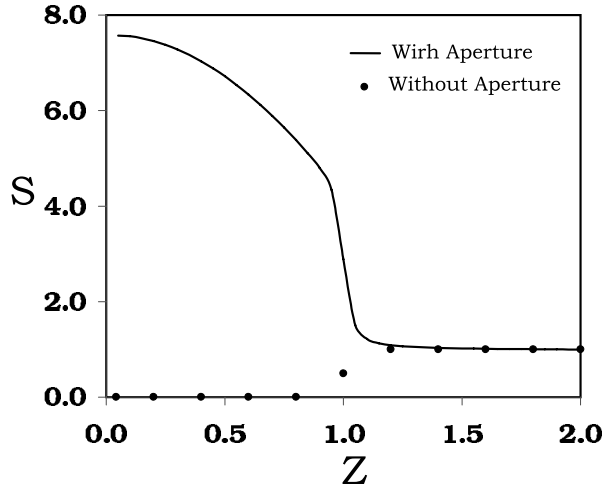

Figure 10 : Total velocity potential versus distance from the center for an acoustically hard open cylinder with an aperture in the top plate subjected to an axially incident plane wave

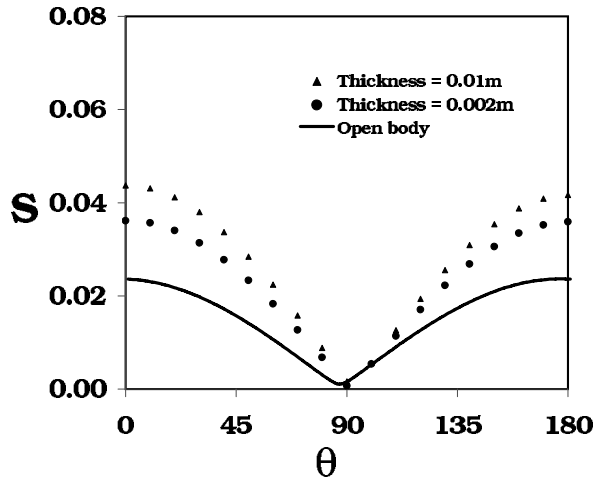

Figure 11 : Scattering cross section versus polar angle for an acoustically hard intersecting plate subjected to an axially incident plane wave

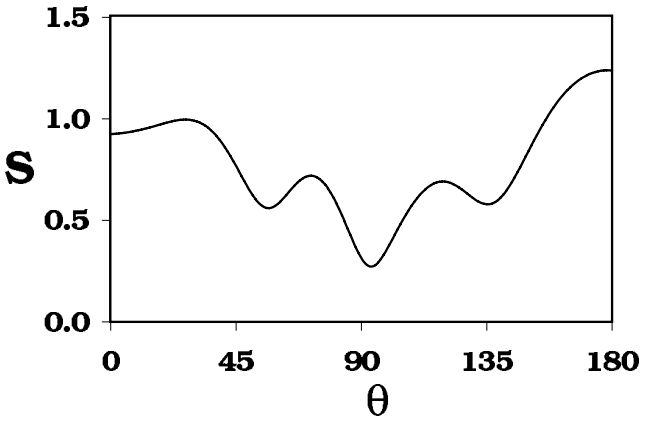

Figure 12 : Scattering cross section versus polar angle for a missile-like structure subjected to an axially incident plane wave

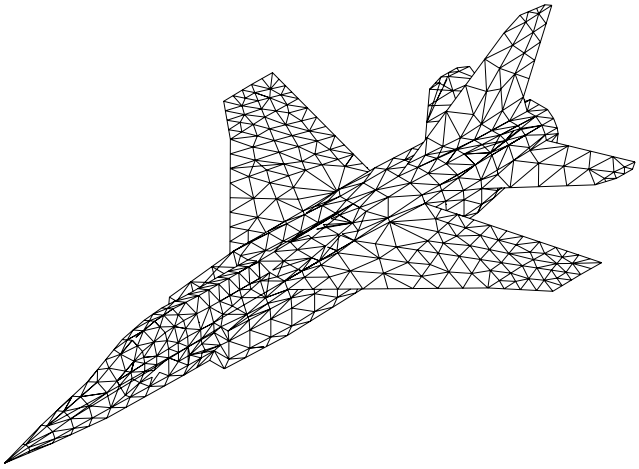

Figure 13 : Triangulated model of an aircraft

the scattering cross section as a function of the elevation angle θ for $\phi = 0^\circ$ and $\phi = 90^\circ$ cuts is presented. Although, only the low-frequency case is considered here, it is obvious that the same algorithm can be used at higher frequencies using a more dense triangulation scheme.

5 Conclusions

In this work, a numerical solution algorithm is presented, based on the method of moments, to the acoustic scattering problem by arbitrarily-shaped, three-dimensional, complex rigid bodies. The governing integral equation is derived using the source distribution concept and the potential theory. Note that the present numerical method is valid at all frequencies, free from the so-called internal resonance problem, and valid for open, closed, and a combination of open/closed bodies. Further, the methodology is simple, efficient and applicable to a large class of problems.

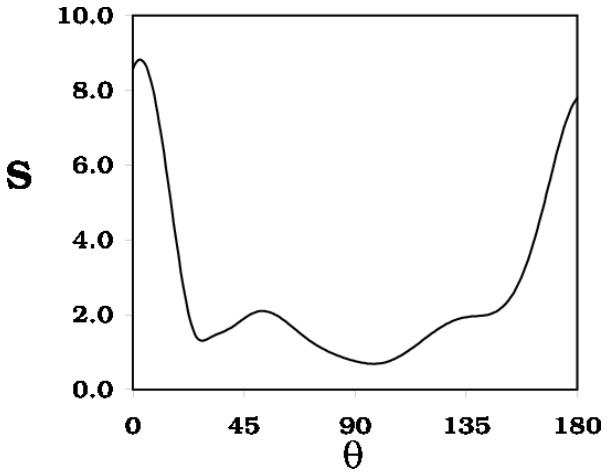

Figure 14 : Scattering cross section versus polar angle for an acoustically hard aircraft subjected to an axially incident plane wave

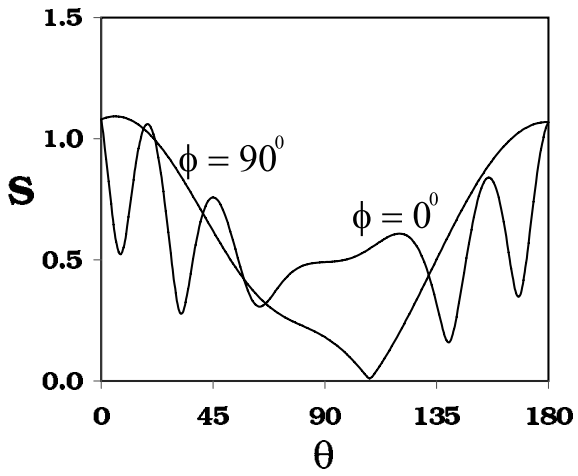

Figure 15 : Scattering cross section versus polar angle for an acoustically hard aircraft subjected to an incident plane wave along the nose direction

References

Benthien, W.; Schenck, H.A. (1997): Nonexistence and Nonuniqueness problems associated with integral equation methods in acoustics, *Computers & Structures.*, 65:295-305.

Bowman, J.J.; Senior, T.B.A.;Uslenghi, P.L.E. (1969): *Electromagnetic and Acoustic Scattering by Simple Shapes*, North Holland Publishing Company.

Burton, A.J.; Miller, G.F. (1971): The application of integral equation methods to the numerical solution of some exterior boundary value problems. *Proceedings of Royal Society*, A323:201-210.

Callsen. S; von Estorff, O.; Zaleski,O. (2004):Direct and Indirect Approach of a Desingularized Boundary Element Formulation for Acoustical Problems,*CMES: Computer Modeling in Engineering & Sciences*, 6(5):421-430.

Chandrasekhar B.;Rao, S.M. (2004a): Acoustic scattering from rigid bodies of arbitrary shape - Double layer formulation, *Journal of Acoustical Society of America*, 115:1926-1933.

Chandrasekhar B.;Rao, S.M. (2004b): Elimination of internal resonance problem associated with acoustic scattering by three-dimensional rigid body, *Journal of Acoustical Society of America*, 115:2731-2737.

Chen, J.T. (1998): On fictitious frequencies using dual series representation, *Mechanics Research Communications*, 25:529-534.

Chen, J.T.; Hong, H.K. (1999), Review of dual boundary element methods with emphasis on hyper-singular integrals and divergent series, *Applied Mechanics Reviews*, 52:17-33.

Chen, J.T.; Kuo, S.R. (2000): On fictitious frequencies using circulants for radiation problems of a cylinder, *Mechanics Research Communications*, 27:49-58.

Chen P.T.; Ju S.H.; Cha K.C. (2000): A symmetric formulation of coupled BEM/FEM solving responses of submerged elastic structures for large degrees of freedom, *Journal of Sound and Vibration*, 233(3):407-422.

Chew, W.C.; Song, J.M.; Cui, T.J.; Velamparambil, S.; Hastriter, M.L.; Hu, B.(2004) Review of Large Scale Computing in Electromagnetics with Fast Integral Equation Solvers,*CMES: Computer Modeling in Engineering & Sciences*, 5(4):361-372.

Ciskowski, R.D.; Brebbia, C.A. (1991): *Boundary Element Methods in Acoustics*, Computational Mechanics Publications, Southampton Boston.

Hammer, P.C.; Marlowe, O.P.; Stroud, A.H. (1956): Numerical integration over simplxes and cones, *Math. Tables Aids Comp*, 10:130-138.

Harrington, R.F. (1968): *Field computation by Method of Moments*, MacMillan.

Hwang, J.Y.; Chang, S.C. (1991): A retracted boundary integral equation for exterior acoustic problem with

unique solution for all wave numbers, *Journal of Acoustical Society of America*, 90:1167-1180.

Kellog, O.D. (1929): *Foundations of Potential Theory*, F. Ungar Publishing Press.

Liu, Y.J.; Rizzo, F.J.(1992): A weakly-singular form of the hyper-singular boundary integral equation applied to 3-D acoustic wave problems. *Computer Methods in Applied Mechanics and Engineering*, 96:271-287.

Liu, Y.J.; Chen, S.H.(1999): A new form of the hyper-singular boundary integral equation for 3-D acoustics and its implementation with C^0 boundary elements. *Computer Methods in Applied Mechanics and Engineering*, 173:375-386.

Maue, A.W. (1949): Zur Formulierung eines allgemeinen Beugungsproblems durch eine Integralgleichung, *Journal of Physics*, 126:601-618.

Mitzner, K.M. (1966): Acoustic scattering from an interface between media of greatly different density. *Journal of Mathematical Physics*, 7:2053-2060.

Qian, Z.; Han, Z.D.; Atluri S.N. (2004a) Directly Derived Non-Hyper-Singular Boundary Integral Equations for Acoustic Problems, and Their Solution through Petrov-Galerkin Schemes. *CMES: Computer Modeling in Engineering & Sciences*, 5(6):541-562.

Qian, Z.Y.; Han, Z.D.; Ufimtsev, P.; Atluri, S.N. (2004b): Non-Hyper-Singular Boundary integral equations for acoustic problems implemented by the collocation-based boundary element method. *CMES: Computer Modeling in Engineering & Sciences*, 6:133-144.

Rao, S. M.; Raju, P.K. (1989): Application of Method of moments to acoustic scattering from multiple bodies of arbitrary shape. *Journal of Acoustical Society of America*, 86:1143-1148.

Reitich, F.; Tamma, K.K. (2004):State-of-the-Art, Trends, and Directions in Computational Electromagnetics, *CMES: Computer Modeling in Engineering & Sciences*, 5(4):287-294.

Reut, Z. (1985): On the boundary integral methods for the exterior acoustic problem. *Journal of Sound and Vibration*, 103:297-298.

Schenck, H.A. (1968): Improved integral formulation for acoustic radiation problems, *Journal of Acoustical Society of America*, 44:41-58.

Tobocman, W. (1984): Calculation of acoustic wave scattering by means of the Helmholtz integral equation I, *Journal of Acoustical Society of America*, 76:595-607.

Tobocman, W. (1984): Calculation of acoustic wave scattering by means of the Helmholtz integral equation II, *Journal of Acoustical Society of America*, 76:1549-1554.

Tobocman, W. (1985): Comparison of the T-matrix and Helmholtz integral equation methods for wave scattering calculations, *Journal of Acoustical Society of America*, 77:369-374.

Ufimtsev, P.Y.(2003): *Theory of Edge Diffraction of Electromagnetics*, Tech Science Press.

Varadan, V.K.; Varadan, V.V. (1980): *Acoustic, Electromagnetic and Elastic wave scattering - Focus on the T-Matrix approach*, Pergamon Press.

Wilton, D.R.;Rao, S.M.; Glisson, A.W.; Schaubert, D.H; Al-Bundak, O.M.; Bulter, C.M. (1984): Potential Integrals for uniform and linear source distributions on polygons and polyhedra domains, *IEEE Transactions on Antennas and Propagation*, 32:276-281

Yan, Z.Y.: Hung, K.C.; Zheng, H. (2003): Solving the hyper-singular boundary integral equation in three dimensional acoustics using a regularization relationship. *Journal of Acoustical Society of America*, 113:2674-2683.

Yan, Z.Y.; Cui, F.S.; Hung, K.C. (2005):Investigation on the Normal Derivative Equation of Helmholtz Integral Equation in Acoustics,*CMES: Computer Modeling in Engineering & Sciences*, 7(1):97-106.